AIAA JOURNAL
Vol. 35, No. 11, November 1997

Scalar Transport in a Swirling Transverse Jet

C. E. Niederhaus,* F. H. Champagne,† and J. W. Jacobs‡
University of Arizona, Tucson, Arizona 85721

The scalar transport in a swirling jet in a crossflow has been investigated in water tunnel experiments. The jet to freestream velocity ratio was varied from 4.9 to 11.1, and the jet swirl numbers ranged from 0 to 0.17. The jet exit Reynolds number was kept at 1.3×10^4 during the experiments. Planar laser-induced fluorescence was utilized to measure planar cross sections of the mean concentration field of the jet up to 68 jet diameters downstream of the exit. The jet penetration depth, half-value radius, and maximum concentration were determined from these concentration fields. For jets without swirl, measured cross-sectional mean concentration distributions have symmetric double-lobed kidney shapes that are consistent with the counter-rotating vortex pair that is known to exist in the far field of the jet. The addition of swirl causes the far-field distributions to become nonsymmetric, with one of the lobes increasing in size and the other decreasing, resulting in a comma shape. Swirl is also observed to decrease jet penetration but not to significantly affect the decay of maximum mean concentration for the range of swirl numbers investigated.

I. Introduction

THE turbulent mixing of jets discharging into a crossflow (shown schematically in Fig. 1) arises in many situations of technological importance. For example, the mixing of jets with and without swirl into a crossflow is important in combustion applications such as jet engines and power plant combustors to enhance fuel efficiency and reduce emissions. Gas turbine combustors also utilize jets in a crossflow to protect their outer casings from hot combustion gases and as dilution jets to lower the combustor exit gas temperature. Other aerospace applications include vertical takeoff and landing aerodynamics and jet injection for the cooling of turbine blades. Jets in a crossflow (also called transverse jets) are also often used for the dispersion of the pollutants in the environment.

The number and diversity of applications has led to a large number of comprehensive studies of transverse jets (see Ref. 1 for a good review of earlier work). Early experiments focused on the determination of the path of the deflected jet,[2,3] whereas later experiments addressed the three-dimensional nature of the flow and the formation and evolution of the vortical structures in a transverse jet.[4,5] However, the vast majority of published work has focused on issues concerning the velocity field.

Remarkably, there is a scarcity of research directed toward scalar transport or mixing, even though the majority of applications of transverse jets require knowledge of the transport of either mass or heat. Patrick[6] utilized an aspirating probe to measure mean concentration profiles in jets seeded with nitrous oxide. Ramsey and Goldstein[7] determined the temperature field for heated jets injected into a freestream at angles of 90 and 35 deg. However, their study focused only on flow near the jet exit and on relatively low values of velocity ratio (from 0.1 to 2.0). Andreopoulos[8] also measured mean temperature profiles and temperature fluctuation statistics in the near field of a slightly heated transverse jet with low velocity ratio (from 0.25 to 2). The flow development for low velocity ratio jets is quite different from that of higher velocity ratio jets.[8] Velocity ratios lower than 4 will not be considered in this study to avoid jet/wall boundary-layer interaction problems.[5]

Broadwell and Breidenthal[9] visually obtained measurements of flame length in experiments that utilized acid-base mixtures and a pH indicator. Kamotani and Greber[10] obtained detailed temperature measurements in both the near and far fields of a heated transverse jet. From these data they determined the jet centerline location, maximum mean temperature, and lateral spread of the jet as functions of the downstream distance. Note, however, that these experiments were conducted with a highly heated air jet (with initial jet temperatures up to 400°F). Thus, the density difference between the jet and the freestream could not be neglected. Smith et al.[11] and Lozano et al.[12] obtained planar laser-induced fluorescence (PLIF) measurements of a transverse air jet with velocity ratios of 5–30. Cross-sectional images are presented of the mean and rms concentration distributions for velocity ratios of 10 and 20 at a few downstream locations.

There have been very few previous experiments focusing on a swirling jet in a crossflow. Kavasaoglu and Schetz[13] measured wall surface pressure distributions and mean velocity measurements with swirl numbers (defined as the axial flux of angular momentum divided by the axial flux of axial momentum times the nozzle radius) of 0.25 and 0.45. Note, however, that these values are estimates computed using their published ratios of azimuthal to axial mean velocity components and graphs in Gupta et al.[14] As with jets without swirl, Kavasaoglu and Schetz's[13] measurements indicate the presence of a pair of counter-rotating vortices in the flow. In addition, they found that in the near field the vortex on the side of the jet where the rotational velocity and the crossflow velocity are in the same direction is closer to the wall than the other vortex. They also determined that swirl decreases the centerline jet penetration. Yoshizako et al.[15] obtained instantaneous concentration measurements in a jet with velocity ratio of 4.0. Most of their experiments were carried out with very high swirl numbers and, therefore, are not comparable to other results. However, at their lowest swirl number ($S = 0.34$), it appears that the change in penetration depth is roughly the same as found by Kavasaoglu and Schetz.[13]

The experiments presented here utilize PLIF to obtain measurements of the mean concentration field of a circular jet, which is injected at a 90-deg angle to a uniform freestream. The PLIF system allowed for the acquisition of cross sections of the mean concentration field at a relatively high spatial resolution, i.e., much higher than previously obtained. This study also differs from previous ones in that the diffusion of the fluorescent dye in water gives a much higher Schmidt number than the Schmidt or Prandtl numbers previously obtained. Measurements were made for jets both with and without swirl to determine the effects of swirl on the scalar transport. The concentration measurements were analyzed to determine jet penetration, maximum concentration, and spreading as a function of velocity ratio, swirl number, and downstream location. When possible, the results are compared to the previous investigations.

II. Experimental Technique

The experiments were conducted in a large (30,000-liter) closed-return water tunnel in the Aerospace and Mechanical Engineering

Received Sept. 30, 1996; revision received June 9, 1997; accepted for publication July 17, 1997.

*Graduate Research Assistant, Department of Aerospace and Mechanical Engineering. Student Member AIAA.
†Professor, Department of Aerospace and Mechanical Engineering.
‡Associate Professor, Department of Aerospace and Mechanical Engineering. Member AIAA.

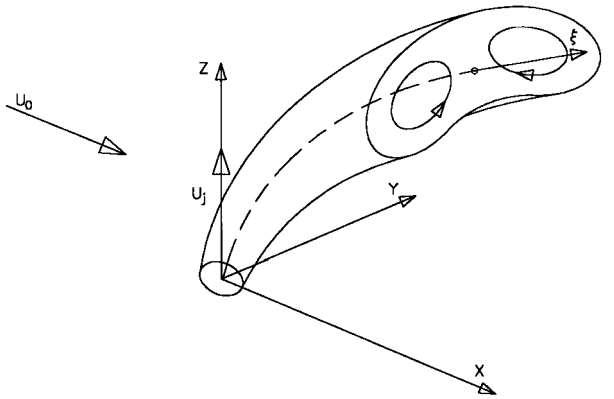

Fig. 1 Coordinate system for a jet in a crossflow.

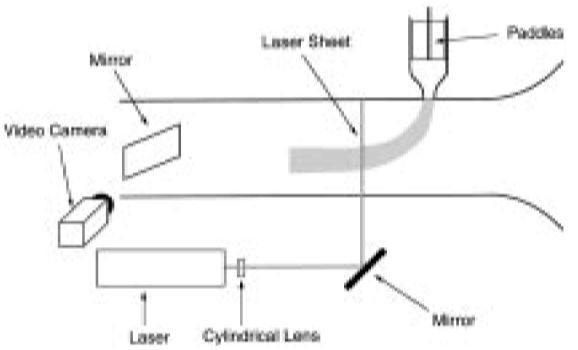

Fig. 2 Schematic of the experimental setup.

Hydrodynamics Laboratory at the University of Arizona. The tunnel has turning vanes, honeycomb flow straighteners, and a 10:1 contraction ratio to ensure flow uniformity and to minimize the turbulence level. The test section is 46 cm high, 71 cm wide, and 4.6 m long. The four test section walls are Plexiglas® to allow for direct visual observation. The circulation for the tunnel is provided by a 7.5-kW motor driven at low revolutions per minute by a microprocessor controller. The speed of the motor is controlled to within ±0.5%. Figure 2 is a schematic of the experimental setup. A 144:1 contraction ratio nozzle, mounted flush with the upper test section wall, forms the jet. The jet is 12.7 mm in diameter and is injected at 90 deg to the freestream. The jet exit is located 60 cm from the end of the tunnel contraction and 10 cm from the tunnel centerline. A centrifugal pump supplies water drawn from the diffuser section of the tunnel into a 81-cm-long plenum chamber located above the nozzle. A rotameter located between the centrifugal pump and the plenum chamber allows monitoring of the jet flow rate.

Throughout the experiments, the jet velocity was kept constant while the tunnel speed was varied to change the velocity ratio. The jet and freestream velocities were measured using a single component frequency-biased laser Doppler anemometer (LDA) operated in back scatter mode. The voltage output of the LDA tracker system was measured using an averaging voltmeter, and the averaged voltage was then used to calculate the velocities. The axial component of the jet exit velocity u exhibited a nearly top hat profile with an average velocity U_j of 1.03 m/s (Fig. 3). The freestream or crossflow speeds U_0 used were 0.093, 0.136, and 0.211 m/s, which produced velocity ratios ($VR = U_j/U_0$) of 11.1, 7.6, and 4.9, respectively. Note that the jet velocity was measured approximately 0.1 jet diameters from the jet exit while the tunnel was not running.

A four-bladed paddle is used in introduce swirl into the jet. The paddle is mounted on a shaft centered inside the jet plenum chamber, and the individual blades are 7.6 cm wide and 15.2 cm long. A stepper motor mounted to the top plate of the plenum is used to rotate the shaft and the paddles. The amount of swirl in a jet can be characterized by the swirl number S, which is normally defined as the axial flux of angular momentum divided by the axial flux of axial momentum (plus pressure) times the nozzle radius:

$$S = \frac{G_\theta}{G_Z D/2} \tag{1}$$

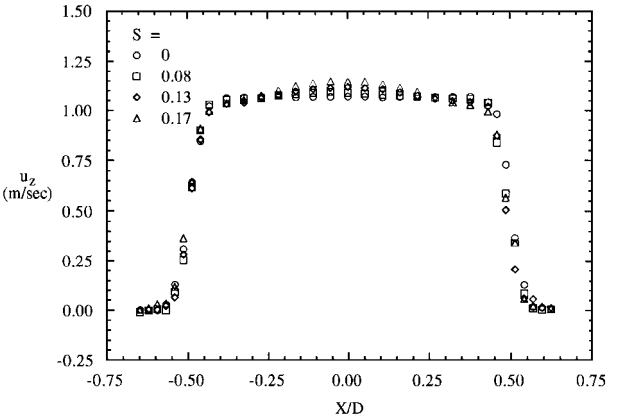

Fig. 3 Radial distribution of jet exit axial velocity.

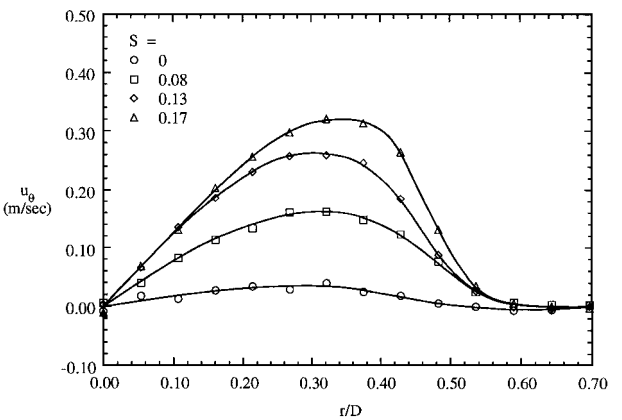

Fig. 4 Radial distribution of jet exit azimuthal velocity.

where

$$G_\theta = \int_0^\infty 2p(ru_Z u_\theta + r\overline{u'_Z u'_\theta})r^2\,\mathrm{d}r \tag{2}$$

$$G_Z = \int_0^\infty 2\pi\left[\rho u_Z^2 + \rho\overline{u_Z'^2} + (p - p_\infty)\right]r\,\mathrm{d}r \tag{3}$$

and u_Z, u_r, and u_θ are the mean velocity components in the Z, r, and θ directions of the cylindrical coordinate system aligned with the jet axis; u'_Z, u'_r, and u'_θ are the fluctuating velocity components; ρ is the density; p is pressure; p_∞ is pressure at infinity; and D is the diameter of the jet exit. Using the radial momentum equation to evaluate pressure in terms of u_θ, and neglecting the Reynolds stresses, Eqs. (2) and (3) can be simplified to

$$G_\theta = \int_0^\infty 2\pi\rho u_Z u_\theta r^2\,\mathrm{d}r \tag{4}$$

$$G_Z = \int_0^\infty 2\pi\rho\left(u_Z^2 - \frac{u_\theta^2}{2}\right)r\,\mathrm{d}r \tag{5}$$

Equations (4) and (5) involve quantities that can be easily measured and, therefore, are utilized to determine S in the present experiments. The azimuthal velocity at the jet exit was also measured using LDA. The paddle rotational speeds utilized to produce swirl were 0, 3.75, 7.5, and 11.25 rpm, which resulted in swirl numbers of 0, 0.08, 0.13, and 0.17, respectively. The measured radial distributions of the axial and azimuthal velocity components at $Z/D = 0.1$ (measured by transversing across the jet at $Y = 0$) are shown in Figs. 3 and 4, respectively. The azimuthal velocity component measurements were found to be axisymetric to within ±4% of U_j.

Fluorescein dye was used with the PLIF system to determine the mixed jet to freestream concentration ratios. The dye is added to the jet flow prior to reaching the plenum chamber. Concentrated dye solution is drawn from a 45-liter container by a diaphragm metering pump. The dye passes through an inline pulse dampener to eliminate

flow surges produced by the metering pump before being injected into the jet supply flow. Further dye homogeneity is accomplished by a mixing tube mounted between the metering pump and the plenum chamber. A 2-W continuous argon ion laser is used as the light source for PLIF. The laser was operated in multiline frequency mode and multiple longitudinal mode to achieve the maximum power output. Light control mode, which maintains a desired power level using a power detector and feedback control circuitry, was used during the experiments. Because drift in the alignment of the laser optics can alter the maximum power output during the day, a setting of 1.5 W was used to ensure that the desired power level was always available. A −12.7-mm-focal-length cylindrical lens attached to the laser output creates the sheet of light necessary for the experiment. The sheet is approximately 400 mm wide and 2.5 mm thick at its half-power points, i.e., the points where the laser intensity is one-half of the maximum laser intensity, when the sheet is in the test section. The laser is placed perpendicular to the tunnel for easy access. The sheet of light is deflected underneath and parallel to the test section by a first surface mirror located 30 cm from the lens. Another mirror, mounted on rails, deflects the sheet upward into the tunnel, perpendicular to the four walls of the test section. Motorization of the second mirror allows quick and accurate placement at different test locations.

Fluorescent images were acquired using a Cohu 4910 series charge-coupled device camera and a VICOM image processing workstation. The camera has 768 × 494 active picture elements with RS-170 video output and was fitted with a 12.5–75-mm-focal-length zoom lens. A mirror mounted inside the test section at a 45-deg angle allows the camera, positioned outside the tunnel, to observe the test section from a perspective directly downstream of the jet. The mirror is located at the end of the test section, 3.7 m (290 jet diameters) from the jet exit and, thus, does not affect the flow region under observation. The images were digitized with a resolution of 512 × 484 by the VICOM workstation at a rate of 30 Hz and then averaged. Most of the final images were the average of 16,384 individual images (approximately 10 min at a 30-Hz sampling frequency). The VICOM has a resolution of 8 bits during acquisition of a single image, but time-averaged images are computed and stored at a resolution of 16 bits. For the mean concentration fields shown, each pixel is 1 mm square, whereas the laser sheet illuminates a volume 2.5 mm thick. The image processing software provided with the VICOM was used to reduce the images into a calibrated form. Programs written in C were then used to calculate the various numerical results presented.

To obtain measurements of dye concentration, it is necessary to calibrate the PLIF system. The intensity of fluorescence is linearly proportional to both the concentration of the dye and the laser sheet intensity at that point. Because the sheet of light produced by the cylindrical lens has a Gaussian intensity distribution, this nonuniformity must be taken into account in the calibration. In addition, the laser sheet intensity is reduced as the sheet passes through the test section due to absorption by the background dye concentration (as given by Beer's law[16]). In the calibration procedure, the tunnel was first doped with a small background dye concentration. After the tunnel water had achieved a uniform concentration, a time-averaged image was taken with the laser on, followed by a time-averaged image taken with the laser off (for noise and background light measurements). The second image was then subtracted from the first, yielding pixel values that were assured to be linearly proportional to the laser intensity at that point. This procedure determines the relative laser sheet distribution in the test section, accounting for both the nonuniform laser sheet and the change in laser intensity due to absorption.

Next, images of the jet, which are corrected for sheet nonuniformity, were obtained by first acquiring an image of the jet from which the background noise level had been subtracted. This result was then divided by the relative laser sheet intensity to yield an image that is linearly proportional to concentration level. Despite precautions taken, the laser sheet distribution changed slightly during the testing, due in part to small changes in the laser optical cavity caused by variations in the temperature of the laser cooling water and in the room. Each vertical column of the image data (roughly corresponding to rays of light in the laser sheet) was corrected for this slight change by a correction factor (typically less than 2%), which assumed that the background concentration level should be uniform.

A change in the background dye concentration during the experiments could also affect the results by changing the laser absorption. Dye was continually being added during the experiment. However, a constant chlorine level in the tunnel slowly bleached out the dye. The net effect was a slight (<15%) change in the background concentration throughout a series of experiments (8–12 individual experiments). The background dye concentration was typically 7×10^{-9} mol/l, which produces a bottom-to-top decrease in background light intensity of approximately 3% (calculated using Beer's law and the height of the test section). Thus, a 15% change in the background concentration produces only a 0.5% change in the laser sheet absorption, which was considered sufficiently small to ignore. Note that this calibration method does not account for the absorption of the laser light as it passes through the jet. However, the jet source concentration of 2.7×10^{-8} mol/l is low enough to ensure that the laser intensity was reduced by no more than 1% as the laser sheet passed through the jet (again computed using Beer's law and the average width of the jet). Again, this intensity difference was considered small enough to ignore.

The final concentration field measurements require knowledge of the concentration of the jet relative to that at the jet source and that of the freestream. For each individual experimental image, the background concentration was measured by filtering out the jet area and taking an average background light intensity. This background concentration was subtracted from the image, yielding a concentration field that shows only the difference due to the jet. This technique accounts for any change in background concentration during a series of experiments. The jet source concentration was determined by first inserting a probe into the tunnel (at the downstream location where the PLIF images were to be taken) through which jet source fluid was injected. A time-averaged image of this probe jet was taken and reduced in the same way as the jet cross-section data. Therefore, dividing the pixel values in the corrected jet images (minus the background value) with those obtained in the potential core region of the probe jet (minus the background value) yields calibrated measurements of the local dye concentration (C) relative to the initial jet dye concentration (C_0).

III. Results and Discussion

The results of the mean concentration field measurements for velocity ratios of 4.9, 7.6, and 11.1 and swirl numbers of 0.0, 0.08, 0.13, and 0.17 will be presented in the form of mean images in Sec. III.A. These concentration measurements were then analyzed to determine the effect of velocity ratio and swirl number on the jet penetration and decay of maximum concentration as a function of downstream location, which will be presented and discussed in Secs. III.B and III.C.

A. Mean Images

Mean concentration field images were obtained at X/D locations of 4, 8, 12, 18, 24, 30, 40, 54, and 68 for the 12 different combinations of VR and S. Images were not obtained for $VR = 11.1$ and $X/D = 68$ because the jet was intermittently hitting the test section floor. Figure 5 shows the collection of images for $VR = 7.6$ and $S = 0$ for all locations tested. The upper wall of the test section, corresponding to $Z/D = 0$, is at the top of each image, and the vertical centerline of the image corresponds to the centerline of the jet ($Y/D = 0$). The field of view for each image is 39.7 × 39.7 cm, or 31.25 × 31.25 jet diameters. Although the images were taken by a camera looking upstream, the images are reversed because the camera viewed the cross section through a mirror located in the test section. Therefore, the images appear as if the vantage point is upstream of the cross-section location. The bar placed below the images is a banded gray-scale indicating the level of concentration difference from the background (C/C_0). White indicates zero difference, whereas each subsequent band of white is an increment of $0.05 \times C_0$. There is also a small negative range of concentration difference shown to indicate the level of error in determining the background concentration. The error in relative concentration (C/C_0) was determined to

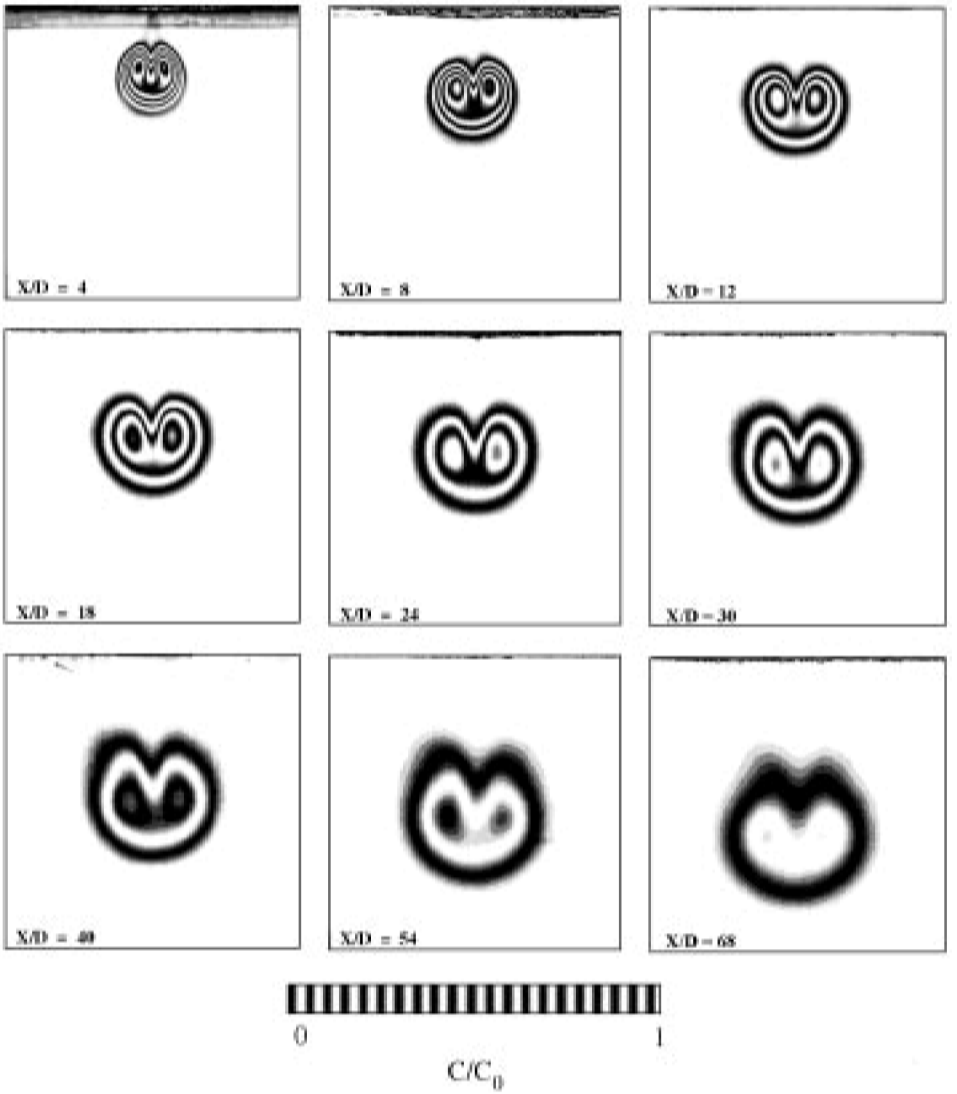

Fig. 5 Mean concentration fields for $VR = 7.6$ with $S = 0$.

be ±6%. The mean concentration images clearly show the classic kidney shape created by the counter-rotating vortex pair, which has been shown to be present in the far field of a jet in a crossflow.[10] Note that the kidney shape is evident even near the jet exit at $X/D = 4$. Based on the observed spreading of the mean concentration images, it also appears that the vortex pair separation is continuously increasing over the entire range of the measurements. The effect of velocity ratio on the jet without swirl can be seen in Figs. 6a, 7a, and 8a, which show the mean concentration fields at $X/D = 24$ with no swirl for $VR = 4.9$, 7.6, and 11.1, respectively. Note that, as the velocity ratio increases, the relative size of the jet increases, a more distinct separation of the two lobes in the concentration field occurs, and the jet has penetrated farther away from the wall.

When swirl is added to the jet flow, the symmetry of the concentration field decreases, and in some cases the kidney shape changes to a comma shape. Figures 6 and 7 show that for velocity ratios of 4.9 and 7.6, the addition of swirl increases the asymmetry of the concentration field at a given X/D up to the maximum swirl number tested of 0.17. The left lobe, where the azimuthal velocity of the entering jet is in the same direction as the crossflow velocity, tends to decrease in size and in maximum concentration with increasing swirl, whereas the right lobe tends to increase in size. For a given swirl number, the magnitude of this effect depends on the velocity ratio. Figure 9, which shows the downstream evolution of the concentration field for $VR = 7.6$ and $S = 0.17$, indicates that the left lobe is closer to the wall than the right lobe in the near field, as observed by Kavasaoglu and Schetz.[13] The left lobe, or tail of the comma, then rotates counterclockwise relative to the right lobe as the jet moves downstream. The left lobe has nearly disappeared far downstream at $X/D = 68$. This rotation may be attributable to the vorticity of the dominant right lobe.

The effect of swirl at $VR = 11.1$ is quite different from the other cases. Figure 8 shows the effect of swirl at $X/D = 24$ for $VR = 11.1$. At low swirl number, there appears to be little difference in shape between the two lobes of the jet, although the left lobe has slightly increased penetration compared with that of the right lobe. However, a larger change in the mean concentration field occurs at $S = 0.17$, where the image assumes the comma shape, and the right lobe becomes larger than the left lobe. It was found that for $VR = 11.1$ and $S = 0.17$ the left lobe rotates counterclockwise relative to the right lobe, the same relative rotation observed at $VR = 4.9$ and 7.6 when swirl was present.

B. Penetration Depth

The mean concentration field data discussed in Sec.III.A were analyzed to determine the effect of velocity ratio and swirl number on the jet penetration as a function of X/D. The penetration depth of the jet is defined here as the Z location of the centroid of the concentration field Z_c, which is determined using

$$\frac{Z_c}{D} = \frac{\int (Z/D) \times (C/C_0)\, \mathrm{d}A}{\int (C/C_0)\, \mathrm{d}A} \tag{6}$$

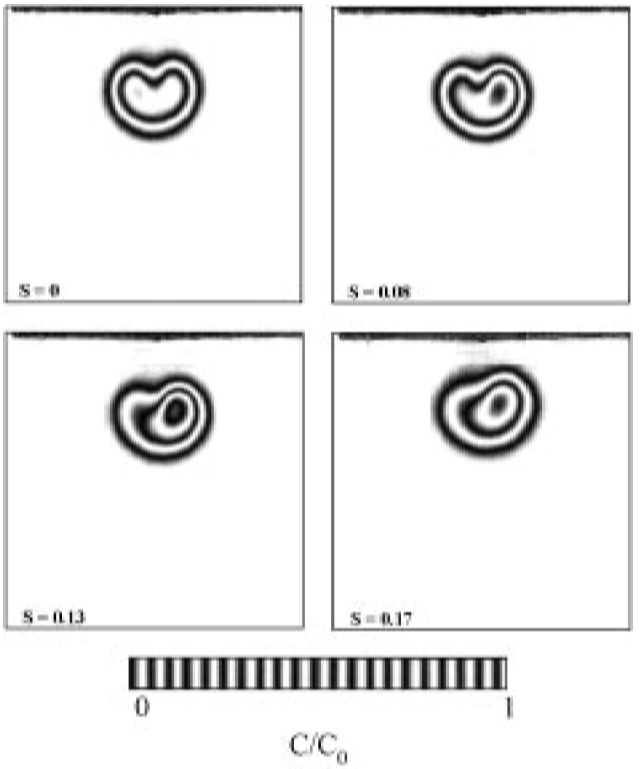

Fig. 6 Mean concentration fields for $VR = 4.9$ at $X/D = 24$.

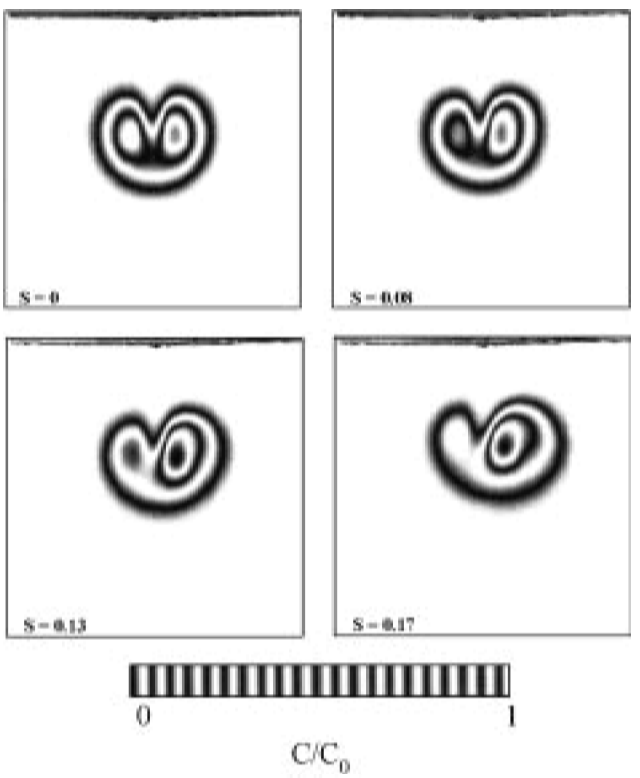

Fig. 7 Mean concentration fields for $VR = 7.6$ at $X/D = 24$.

Pratte and Baines[3] used momentum considerations (assuming that the density of the jet equals that of the freestream) to show that the penetration depth as measured from velocity field data should collapse onto a single curve using lengths nondimensionalized by $VR \times D$. Figure 10 is a plot of $Z_c/(VR \times D)$ vs $X/(VR \times D)$ for the nonswirl case, which shows the concentration field data to collapse reasonably well (the error of the mean for these measurements, estimated by comparing data taken under identical conditions but on different days, is less than $\pm 1.3\%$). Kamotani and Greber,[10] on the other hand, present a best fit curve for the nondimensional Z location of the point of maximum mean centerline temperature Z_{cl} in their experiments. They assumed that the equation for the maximum centerline location was of the form

$$Z_{cl}/D = \text{const} \times J^a \times (\rho_j/\rho_0)^b \times (X/D)^c \qquad (7)$$

where J is the ratio of momentum flux per unit area for the jet to that of the freestream. The velocity ratio values of 4.9, 7.6, and 11.1 in the present experiment correspond to J values of 23.8, 57.3, and 123, respectively. Note that there is no theoretical basis to justify the form of this equation and, thus, there is no reason to assume that their best fit equation should apply outside the range of J they investigated, $15 \leq J \leq 60$. Figure 11 shows the nondimensional Z location of the point of maximum concentration along the centerline of the jet for the nonswirl case, together with the best fit curve obtained by Kamotani and Greber[10] for maximum centerline temperature. The present data and the curve given by Kamotani and Greber show excellent agreement for velocity ratios of 4.9 and 7.6 (which correspond to momentum ratios of 23.8 and 57.3). Although the data for $VR = 11.1$ ($J = 123$) differs from their curve, it lies well outside the range of momentum ratios they investigated.

Swirl has a noticeable effect on penetration depth for a velocity ratio of 4.9 and 7.6, as shown in Fig. 12. The best fit curves shown are power law fits of the form $a(X/D)^b$. At these velocity ratios, the addition of a small amount of swirl ($S = 0.08$) slightly increases the penetration depth relative to the no swirl condition. However, at higher swirl numbers, the penetration depth decreases relative to the nonswirl case, which may be attributed to the weakened mutual induction effect between the asymmetrical vortex pattern as compared to the symmetrical one. For the velocity ratio of 11.1, however, the effects of adding swirl are much reduced and quite different, as shown in Fig. 12. In this case, the addition of swirl slightly increases the centroid penetration depth until $S = 0.13$. At $S = 0.17$, the penetration depth decreases relative to that for $S = 0.13$ but is still greater than that for $S = 0$. Also note that it is when $S = 0.17$ that the mean concentration field first showed a marked asymmetry for this velocity ratio (Fig. 8). The circulation in the counter-rotating vortex pair (as defined by the circulation of one vortex[5]) is considerably increased at this higher VR such that it takes a higher swirl number to affect the vortex pattern. Kavasaoglu and Schetz[13] found

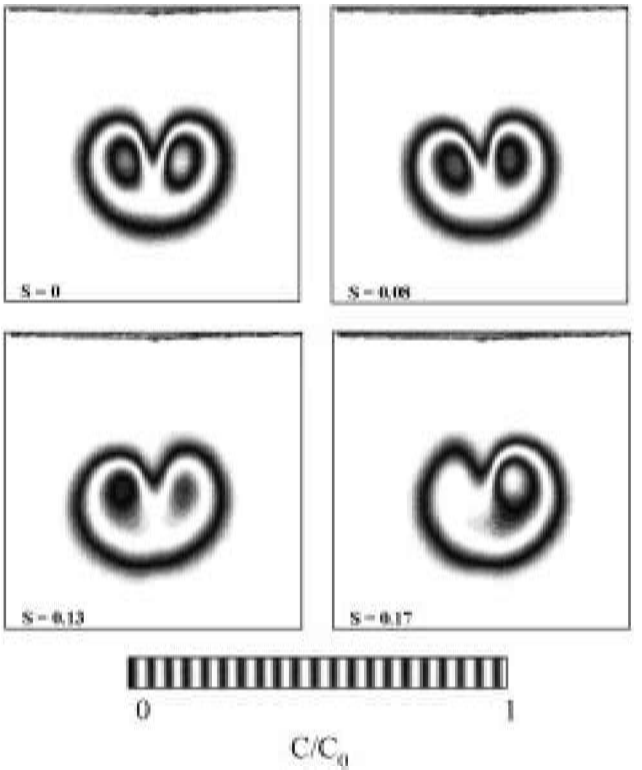

Fig. 8 Mean concentration fields for $VR = 11.1$ at $X/D = 24$.

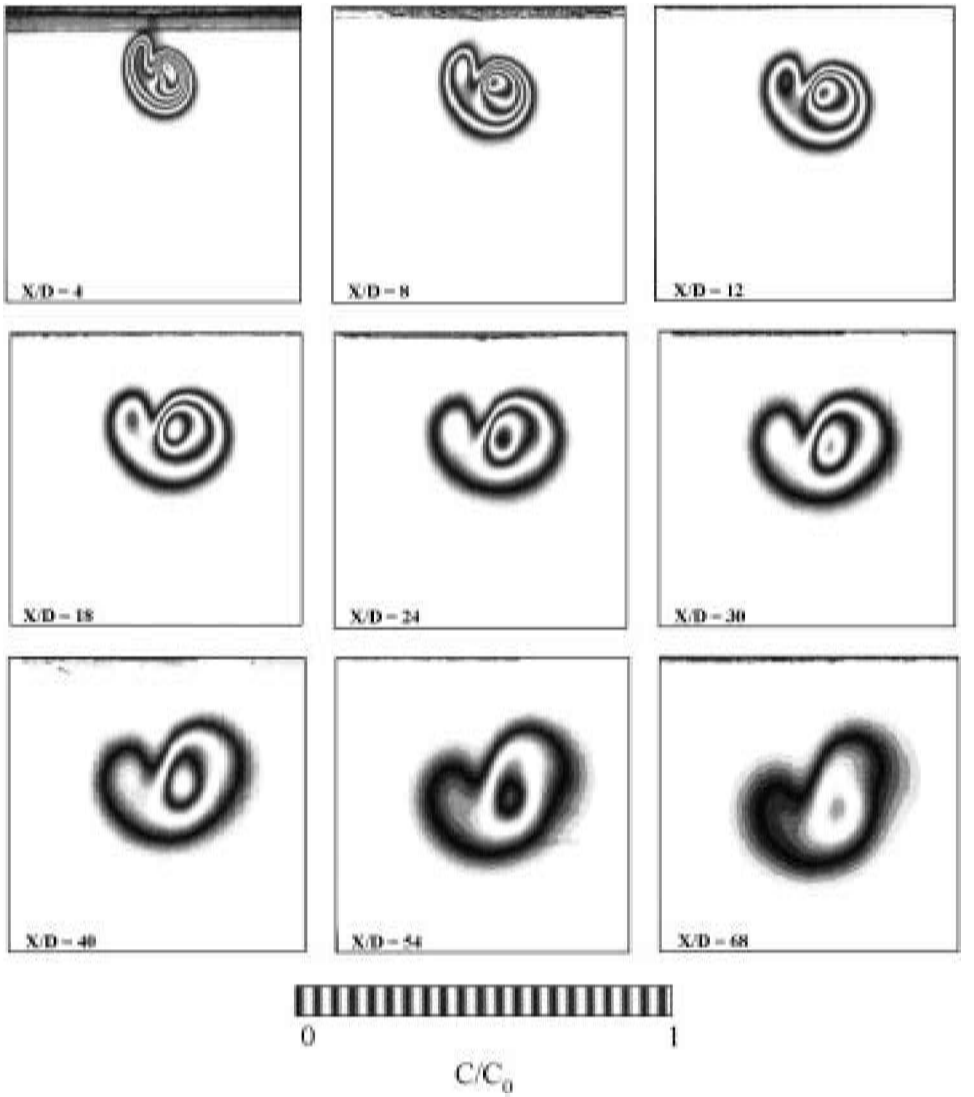

Fig. 9 Mean concentration fields for $VR = 7.6$ with $S = 0.17$.

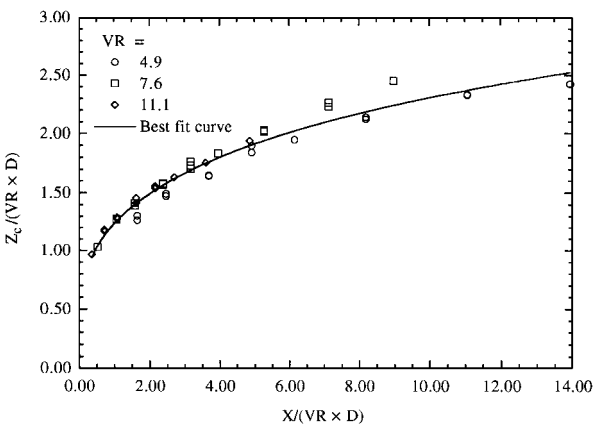

Fig. 10 Centroid penetration depth without swirl.

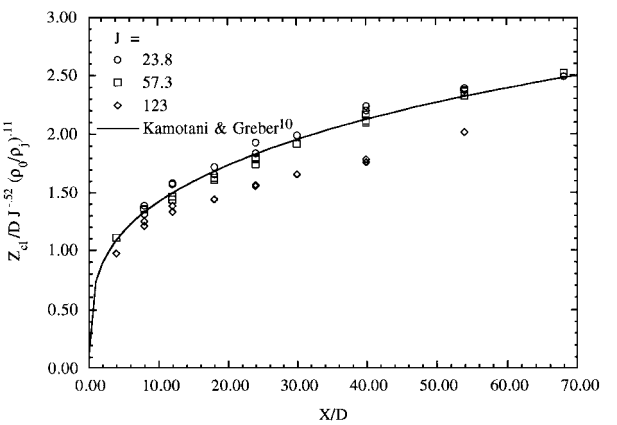

Fig. 11 Centerline penetration depth without swirl.

that for $VR = 4.0$ the penetration depth for the maximum centerline jet velocity at $X/D = 6$ had decreased by 6% for $S = 0.25$ and by 30% for $S = 0.45$, when compared to their nonswirl case. The present results for the concentration field indicate a 5% decrease in the penetration of the mean concentration centroid for $S = 0.17$, when compared to the nonswirl case. These results agree reasonably well considering the large differences between the two experiments.

C. Decay of Maximum Concentration

The maximum concentration of the jet at a fixed downstream location was determined for all of the mean concentration fields measured. When possible, two local concentration maxima were measured, one in the right half of the jet, the other in the left. At high swirl numbers, the concentration distribution of the jet has a comma shape and, thus, there is only one local maximum. Furthermore, the shape in the no swirl case is not always exactly symmetrical (as past

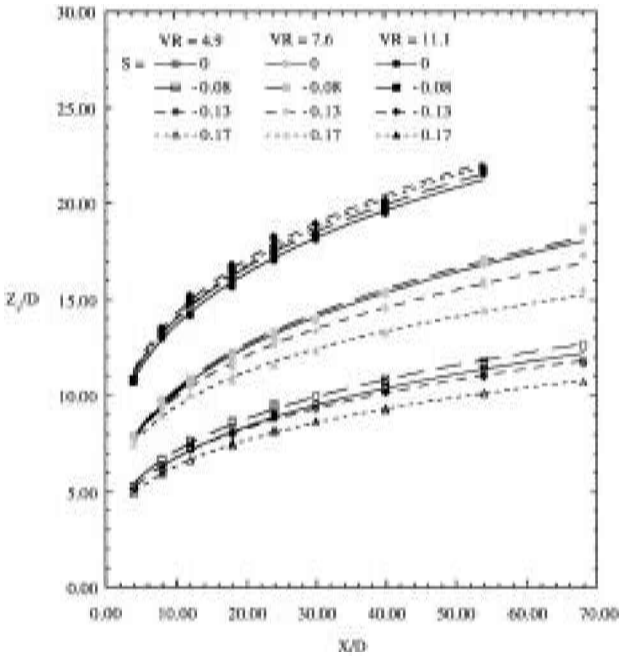

Fig. 12 Centroid penetration depth vs *X/D*.

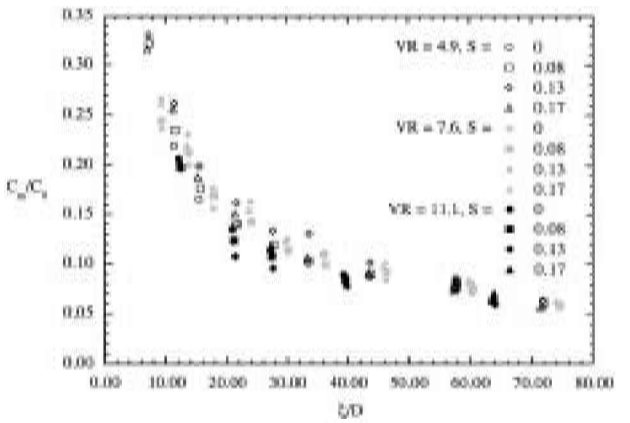

Fig. 13 Maximum mean concentration vs arclength.

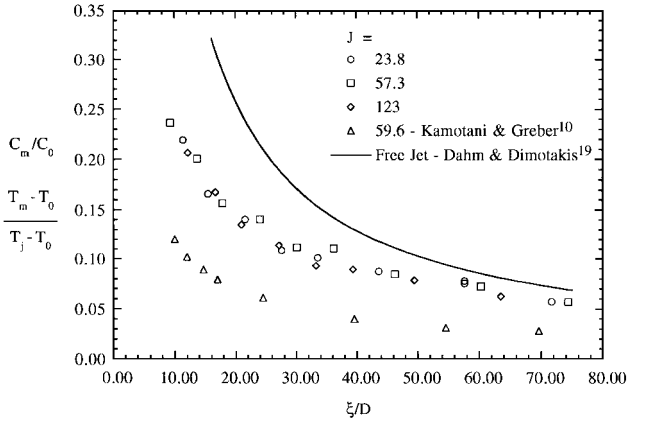

Fig. 14 Maximum mean concentration without swirl vs arclength.

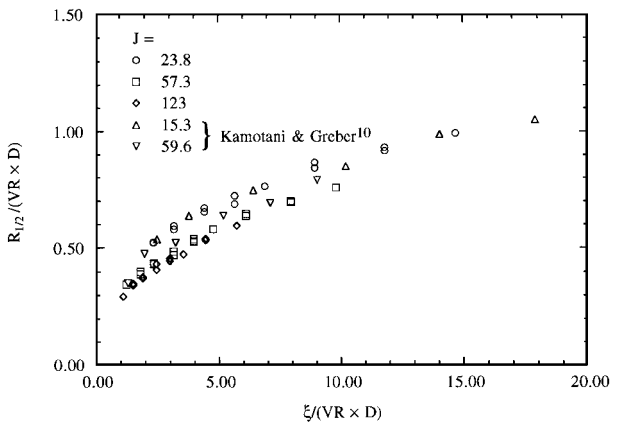

Fig. 15 Half-value radius without swirl vs arclength.

experimentershave also found), resulting in the two lobes not having the same maximum concentration. The largest difference between the two maxima observed in the present experiments was 12%. Because of this asymmetry and the fact that swirl would often lead to only one local maximum, only the absolute maximum concentration in each image is plotted.

Figure 13 shows the maximum concentration (C_m/C_0) vs arclength along the centroid of concentration (ξ/D), for all of the velocity ratios and swirl numbers tested ($VR = 4.9$, 7.6, and 11.1; $S = 0$, 0.08, 0.13, and 0.17). The arclength was computed by numerically integrating the distance along the best fit curve for Z_c/D. The reasonably tight grouping of the data in this plot indicates that swirl does not have a large measurable effect on the maximum concentration, at least for the range of swirl numbers investigated here. The maximum concentrations for the three velocity ratios without swirl as a function of arclength are shown in Fig. 14. The collapse of these data indicates that the maximum concentration is only a function of arclength (at least in the far field) and is, therefore, nearly independent of velocity ratio in the range tested. Also shown in this plot are the normalized maximum temperature measurements of Kamotani and Greber.[10] Note that Kamotani and Greber's results are approximately one-half of the equivalently normalized concentration measurements from the present investigation.

The decay of the maximum concentration with X is related to the rate of spread of the jet. To provide a measure of the lateral spread of the jet, the half-value radius ($R_{1/2}$) is used, which is defined as the radius of a circle that would contain the same area as that part of the jet above a concentration level $C/C_m = 0.50$. Figure 15 shows the downstream variation of $R_{1/2}$ vs arclength for the nonswirl cases with $J = 23.8$, 57.3, and 123. Also shown are the data of Kamotani and Greber.[10] $R_{1/2}$ and ξ have been scaled in this plot using the same scaling as used in Fig. 10. Although there appears to be a slight dependence on the momentum ratio, this scaling collapses the jet spread data reasonably well. Note also that Kamotani and Greber's results agree very well with the present measurements.

Kamotani and Greber's temperature measurements and the equivalently normalized concentration measurements from the present investigation differ by a factor of two. However, the measurements of jet spread from both investigations are in excellent agreement. These trends extend out to $X/D = 70$, where the streamwise velocity component should approximately equal the freestream velocity.[17] If the distributions of temperature and species concentration were similar, then the disagreement in maximum scalar concentration suggests that the conservation of species or energy is not satisfied in one of the two experiments. In the present experiments, conservation of species was verified by comparing the inlet species flux at the jet orifice ($C_0 U_j A_j$, where A_j is the jet exit area) with the flux of species across a plane far downstream of the jet inlet. The flux of species in far-field cross sections was estimated by assuming that the axial velocity in the jet is equal to U_0 and integrating the mean concentration distributions over a cross section in the far field. For $X/D > 50$, the results agreed to within 10, 15, and 25% for $VR = 11.1$, 7.6, and 4.9, respectively, thereby verifying that the present data satisfy the conservation of species (at least to within 25%). The difference between the present maximum concentration measurements and the results of Kamotani and Greber can possibly be attributed to lack of similarity between the concentration and temperature distributions, or the effects of large density differences in the near field for the heated jet.

The far downstream species flux estimates for the preceding analysis were always greater than the jet inlet values, which is to be expected if the actual jet axial velocity is slightly lower than U_0. Fric

and Roshko[5] pointed out that the transverse jet cannot be considered as a free shear flow. They showed that the crossflow boundary layer separates near the downstream side of the jet and forms a system of vortices in the wake of the transverse jet. The boundary fluid becomes entrained into these wake vortices, which extend from the wall to the deflected transverse jet. This funneling of crossflow boundary fluid into the wake structures must result in a momentum loss of the jet flow, which would be evident in the far field. This effect would be more prevalent at lower velocity ratios, possibly explaining the higher disagreement in the species flux estimate at $VR = 4.9$.

For a freejet at high Reynolds number, where the mixing is turbulence dominated, scalar transport is independent of Prandtl number or Schmidt number,[18] and one would expect similar results for a transverse jet. Shown in Fig. 16 are the centerline normalized concentration measurements of Dahm and Dimotakis[19] for a water jet with a Reynolds number of 5×10^3. Comparison with the present results indicates that in the near field, a transverse jet is a better mixer than a freejet. However, in the far field the maximum mean concentration for a transverse jet and a freejet are closer in value.

IV. Conclusions

Measurements of the mean concentration field in the far field of a jet in a crossflow were obtained for velocity ratios of 4.9, 7.6, and 11.1, and swirl numbers of 0, 0.08, 0.13, and 0.17. The results without swirl were qualitatively consistent with previously published data. The kidney-shaped structures observed for high velocity ratios are similar to temperature and species concentration data obtained in previous experiments. At a fixed downstream location it was observed that the lobes of the kidney shape become more pronounced as the velocity ratio is increased. Scalar penetration depth measured along the jet centerline and the half-value radius closely agree with those obtained by Kamotani and Greber.[10] However, measurements of the maximum concentration at a given downstream location are considerably larger than those obtained for temperature by Kamotani and Greber.

The effect of swirl on the jet was found to be complex and dependent on the velocity ratio. The addition of small amounts of swirl to transverse jets with low to moderate velocity ratios was observed to decrease the penetration depth (up to a maximum of 20%) and to transform the symmetric kidney-shaped mean concentration field to that of a nonsymmetrical comma shape, with the degree of asymmetry increasing as the swirl number increased. This effect was significantly reduced at higher velocity ratios. On the other hand, the addition of swirl was found to not significantly affect the decay of maximum concentration.

Acknowledgments

This research was supported by the National Science Foundation under Grant No. CTS-9057039. The authors are grateful to G. Hopkins for help in building the experimental setup and to R. James for his valuable assistance in conducting the laser Doppler anemometer measurements.

References

[1]Rajaratnam, N., *Turbulent Jets*, Elsevier Scientific, Amsterdam, 1976, Chap. 9.

[2]Keffer, J. F., and Baines, W. D., "The Round Jet in a Cross-Wind," *Journal of Fluid Mechanics*, Vol. 15, Pt. 4, 1963, pp. 481–496.

[3]Pratte, B. D., and Baines, W. D., "Profiles of the Round Turbulent Jet in a Cross Flow," *Journal of the Hydraulics Division ASCE*, Vol. 92, 1967, pp. 53–64.

[4]Fric, T. F., "Structure in the Near Field of the Transverse Jet," Ph.D. Thesis, Graduate Aeronautical Labs., California Inst. of Technology, Pasadena, CA, April 1990.

[5]Fric, T. F., and Roshko, A., "Vortical Structure in the Wake of a Transverse Jet," *Journal of Fluid Mechanics*, Vol. 279, Nov. 1994, pp. 1–47.

[6]Patrick, M. A., "Experimental Investigation of the Mixing and Penetration of a Round Turbulent Jet Injected Perpendicularly into a Transverse Stream," *Transactions of the Institution of Chemical Engineers*, Vol. 45, No. 1, 1967, pp. T16–T31.

[7]Ramsey, J. W., and Goldstein, R. J., "Interaction of a Heated Jet with a Deflecting Stream," *Journal of Heat Transfer*, Vol. 93, Nov. 1971, pp. 365–372.

[8]Andreopoulos, J., "Heat Transfer Measurements in a Heated Jet-Pipe Flow Issuing into a Cold Cross Stream," *Physics of Fluids*, Vol. 26, No. 11, 1983, pp. 3201–3210.

[9]Broadwell, J. E., and Breidenthal, R. E., "Structure and Mixing of a Transverse Jet in Incompressible Flow," *Journal of Fluid Mechanics*, Vol. 148, Nov. 1984, pp. 405–412.

[10]Kamotani, Y., and Greber, I., "Experiments on a Turbulent Jet in a Cross Flow," *AIAA Journal*, Vol. 10, No. 11, 1972, pp. 1425–1429.

[11]Smith, S. H., Hasselbrink, E. F., Mungal, M. G., and Hanson, R. K., "The Scalar Concentration Field of the Axisymmetric Jet in Crossflow," AIAA Paper 96-0198, Jan. 1996.

[12]Lozano, A., Smith, S. H., Mungal, M. G., and Hanson, R. K., "Concentration Measurements in a Transverse Jet by Planar Laser-Induced Fluorescence of Acetone," *AIAA Journal*, Vol. 32, No. 1, 1993, pp. 218–221.

[13]Kavasaoglu, M. S., and Schetz, J. A., "Effects of Swirl and High Intensity Turbulence on a Jet in a Crossflow," *Journal of Aircraft*, Vol. 26, No. 6, 1989, pp. 539–546.

[14]Gupta, A. K., Lilley, D. G., and Syred, N., *Swirl Flows*, Abacus, Kent, England, UK, 1984, Chap. 1.

[15]Yoshizako, H., Yoshida, K., and Akiyama, L., "Diffusion of a Jet Injected Perpendicularly into a Uniform Cross Flow," *Transactions of the Japanese Society of Mechanical Engineering*, Vol. 57, 1991, pp. 354–359.

[16]Walker, D. A., "A Fluorescence Technique for Measurement of Concentration in Mixing Liquids," *Journal of Physics E: Scientific Instruments*, Vol. 20, No. 2, 1987, pp. 217–224.

[17]Fearn, F., and Weston, R. P., "Vorticity Associated with a Jet in a Cross Flow," *AIAA Journal*, Vol. 12, No. 12, 1974, pp. 1666–1671.

[18]Dowling, D. R., and Dimotakis, P. E., "Similarity of the Concentration Field of Gas-Phase Turbulent Jets," *Journal of Fluid Mechanics*, Vol. 218, Sept. 1990, pp. 109–141.

[19]Dahm, W. J. A., and Dimotakis, P. E., "Mixing at Large Schmidt Number in the Self-Similar Far Field of Turbulent Jets," *Journal of Fluid Mechanics*, Vol. 217, Aug. 1990, pp. 299–330.

F. W. Chambers
Associate Editor